Oriented Crystallization Induced by Uniaxial Drawing from Poly(tetrafluoroethylene) Melt

Takashi Morioka,[†] Masaki Kakiage,[†,‡] Takeshi Yamanobe,[†] Tadashi Komoto,[†] Yoshiaki Higuchi,[§] Hiroki Kamiya,[§] Kiyotaka Arai,[||] Syozo Murakami,[#] and Hiroki Uehara*[,†]

Department of Chemistry, Gunma University, Kiryu, Gunma 376-8515, Japan, R & D Division, Asahi Glass Co., Ltd., Ichihara, Chiba, 290-8566, Japan, Central Laboratory, Asahi Glass Co., Ltd., Yokohama, Kanagawa, 221-8755, Japan, and Heian Jogakuin University, Takatsuki, Osaka 569-1092, Japan

Received August 22, 2007; Revised Manuscript Received October 2, 2007

ABSTRACT: The melt-drawing behavior of poly(tetrafluoroethylene) (PTFE) with ultrahigh molecular weight (UHMW) was analyzed using in situ measurements composed of stress−strain curves and wide-angle X-ray diffraction with synchrotron radiation. The stress−strain behavior of the melt-drawing of UHMW−PTFE was quite different from that of the solid drawing. In particular, the former exhibited a plateau stress region, followed by a rapid increase in stress with strain. No crystalline reflection appeared in the plateau stress region. However, oriented crystallization was observed in the later strain-hardening region. Correspondingly, the resultant mechanical properties and transparency of the melt-drawn films are much better than those of the solid-drawn films. Optimizing the melt-drawing conditions elongated the plateau stress region, which successfully achieved further property development. The effects of sample MW on melt-drawing behavior and resultant properties were also discussed. The lower MW film produced a longer plateau region. Subsequent oriented crystallization in the strain-hardening region also exhibited a rapid increase of the crystalline reflection intensity, compared to that for the higher MW film. However, the resultant properties were lower than those for the higher MW film, due to the higher content of the chain ends, even if a higher resultant crystallinity was achieved.

Introduction

Poly(tetrafluoroethylene) (PTFE) has excellent thermal stability,[1] electrical insulation,[2] friction coefficient,[3] and biocompatibility.[4] These properties are desirable for various membrane applications, with PTFE having been adopted worldwide as a base material. Thus, its crystalline structure has been still analyzed both in various methodological[5−9] and recent modeling approaches.[10,11] However, its high melt viscosity is a disadvantage, which leads to poor processability. Therefore, blending with low molecular weight components,[12] including oligomers or various plasticizers,[13−14] has been investigated. Unfortunately, the compound properties are poorer than those of the base PTFE having the higher molecular weight.

In contrast, PTFE reactor powder can be used effectively to prepare high-performance film, even for higher molecular weight materials without any of the above impurities, due to the less entangled state of its as-polymerized morphology.[15−18] In order to maintain this reactor power state within the prepared film, the processing temperature is kept below the melting temperature (T_m). The obtained film is brittle because of the poorer adhesion between powder particles. For further property development by the ultradrawing process, solid-state coextrusion,[15,16,18] which extrudes the assembly of the film sandwiched between halves of a PTFE billet, is required. Subsequent tensile drawing below T_m results in a tensile strength of 400 MPa,[15,16,18] but such combination of different orientation techniques leads to complex processing.

* Corresponding author. E-mail: uehara@chem-bio.gunma-u.ac.jp.
[†] Department of Chemistry, Gunma University.
[‡] Research Fellow of the Japan Society for the Promotion of Science.
[§] R & D Division, Asahi Glass Co., Ltd.
[||] Central Laboratory, Asahi Glass Co., Ltd.
[#] Heian Jogakuin University.

Nevertheless, the high melt viscosity of PTFE could be advantageous if tensile drawing could be induced in the molten state. The higher viscosity means a longer relaxation time, so the molecular orientation would be retained when the deformation time scale exceeds the chain relaxation during drawing from the melt. In fact, in a series of our recent studies,[19−21] we clarified that ultrahigh molecular weight polyethylene (UHMW−PE), having a high melt viscosity similar to PTFE, is ultradrawable into the high-performance materials from the molten state, as it passes through the oriented crystallization phenomenon. Structural development during the melt-drawing process of UHMW−PE has been analyzed by in situ X-ray measurements using a high-brilliance synchrotron radiation source.[22−24] This measurement technique is suitable for detecting the rapid structural change during processing, due to its higher time-resolution in seconds.[25−31] The obtained results of our in situ analyses for melt-drawing of UHMW−PE suggested that disentanglement of the molecular chains takes place in the early stage of processing, but it induces the subsequent oriented crystallization.[22−24] Corresponding to the unique deformation mechanisms of the melt-drawing processing, the resultant film exhibited a superior tensile strength exceeding 800 MPa.[32] This is less than that for the reactor powder processing performed below T_m for the same UHMW−PE material, but the associated melt-drawing process is composed of only one step, uniaxial tensile drawing from the melt. Combination of molecular disentanglement and the subsequent oriented crystallization during melt-drawing is a key for desirable property development, despite the simple procedure, compared with solid-state drawing from the reactor powder state, which requires several processing steps.

Following this concept of melt-drawing using high melt viscosity of the applied material, we chose UHMW−PTFEs

10.1021/ma071898g CCC: $37.00
Published on Web 11/30/2007

because they have MW exceeding 10^6. The initial film was prepared by the usual compression molding above T_m and then drawing in the solid or molten state. Structural changes occurring during uniaxial drawing processes were subjected to in situ analysis composed of stress/strain curves and wide-angle X-ray diffraction (WAXD) measurements made with synchrotron radiation at SPring-8, Japan. The drawing conditions, including the drawing temperature and rate, were optimized in terms of the resultant tensile properties and transparency of the drawn film. These properties are especially important for membrane applications, which is one of the typical uses of PTFE. The melt-drawing behavior and resultant properties for UHMW−PTFE having different MWs were also compared.

Experimental Section

Materials. Three UHMW−PTFE powders with number-average MW (M_n) of 2×10^6, 4×10^6 and 1×10^7 were supplied by Asahi Glass Co., Ltd. These sample M_ns were estimated from their heats of crystallization detected by differential scanning calorimetry (DSC) measurements.[33] The powder sealed in a DSC pan was melted at 380 °C and cooled at a rate of 10 °C/min.

Film Preparation. These as-received powders were compression molded into films at 370 °C and 30 MPa for 10 min, followed by slow cooling to room temperature. The T_m of the sample films were 328 °C for $M_n = 1 \times 10^7$, and 330 °C for $M_n = 2 \times 10^6$ and 4×10^6, as estimated by DSC measurement described later. The drawing specimens were cut from these films in dumbbell shapes, with the straight region 4 mm wide and 12.5 mm long.

In Situ WAXD Analysis. Each specimen was set in a high-temperature extension device[34,35] installed on SPring-8 beamline BL40B2 and tensile-drawn at various temperatures from 25 to 370 °C. The cross-head speed (CHS) of drawing was always 24 mm/min. Strain was calculated from the drawing time and the initial length of the film. Stress/strain curves and WAXD patterns were simultaneously recorded during drawing. A synchrotron beam with a wavelength of 1.00 Å was applied. A 0.3-mm-diameter beam was radiated at the center of the dumbbell sample, where the measurement temperature was detected by thermocouples placed less than 1 mm away from the sample surface. The exposure time was 0.2 s for each in situ pattern recorded with a time interval of 5.5 s for data storage. A blank pattern for air scattering was also recorded without the sample set but at the measured temperature. The obtained air-scattering data was subtracted from each in situ pattern recorded during the sample deformation.

Resultant Property Measurements. The resultant tensile properties of the drawn films were measured using a universal tensile tester (Orientec RTC-1325A) at room temperature and at a strain rate of 0.6 min^{-1}. The tensile strength of each drawn film was calculated from the maximum stress just before breaking of the sample. The light transmittance of the drawn film was measured at a wavelength of 430 nm using a UV/vis spectrometer (Shimazu Corporation UV3000) to evaluate the transparency of the film. The absorption coefficient per 1 μm was calculated from the measured transmittance and film thickness. The resultant crystallinities of the drawn films were estimated from the fusion heats measured by DSC scans. These DSC measurements were made using Seiko DSC-220C operated from room temperature to 400 °C at a heating rate of 10 °C/min under nitrogen gas flow. Both temperature and heat flow were calibrated by indium and tin standards. An enthalpy of 70 J/g was used as that of the perfect crystals of PTFE.[36]

Results and Discussion

Comparison of Solid- and Melt-Drawing Behavior. First, the effect of drawing temperature was examined for the film prepared from $M_n = 1.0 \times 10^7$ powder. The obtained stress/strain curve exhibited a significant dependence on drawing temperature (Figure 1). The curve shape gradually changed until 350 °C. Namely, the draw stress gradually decreases with

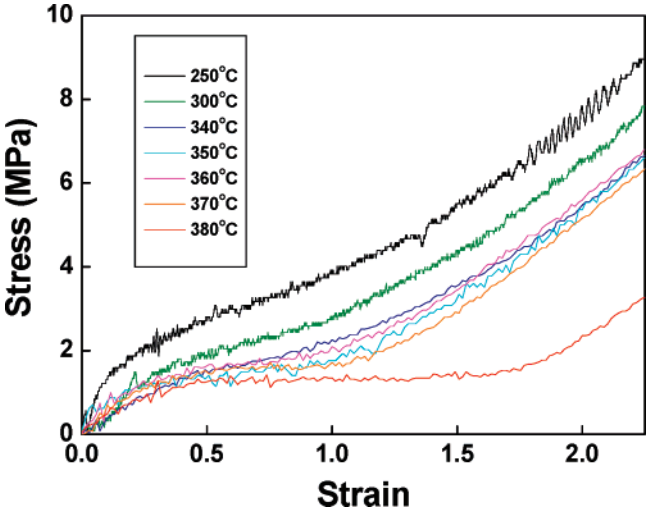

Figure 1. Stress/strain curves recorded at 250 to 380 °C during drawing of the UHMW−PTFE films prepared from $M_n = 1.0 \times 10^7$ powder.

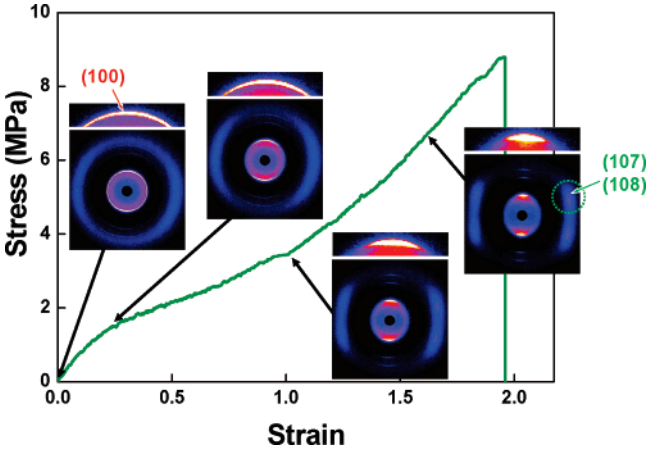

Figure 2. Stress/strain curve recorded at 300 °C with the corresponding change of in situ WAXD patterns for the films prepared from $M_n = 1.0 \times 10^7$ powder. Draw direction on WAXD patterns is horizontal. Enlarged images of the crystalline reflection regions were attached on the upper side.

increasing drawing temperature. In contrast, the characteristic plateau stress region exhibiting a constant stress level was observed beyond 360 °C. Such a plateau stress region has also been observed during melt-drawing of UHMW−PE.[22−24] This stress/strain behavior suggests that solid-drawing and melt-drawing are distinguishable based on the presence of a plateau region for our UHMW−PTFE film as well.

Next, the structural changes during melt-drawing and solid-drawing were compared by analyzing in situ WAXD patterns. Figures 2 and 3 present stress/strain curves observed at 300 and 370 °C with a series of WAXD patterns recorded at the corresponding strains. For solid-drawing, an unoriented ring of the pseudo-hexagonal (100) reflection was observed before drawing. Upon starting the draw, this reflection gradually concentrated on the equator with increasing strain. The higher-order reflections of (107) and (108) also oriented on the first layer line. These mean that deformation proceeds in the crystalline state during drawing at this temperature and that the molecules gradually orient along the drawing axis with increasing strain. However, the chain orientation, estimated from the azimuthal distribution of the reflection, was lower than that observed during melt-drawing, as will be discussed later. This difference in chain orientation is opposite to drawing stress level, which was higher for solid-drawing. In contrast, drawing is

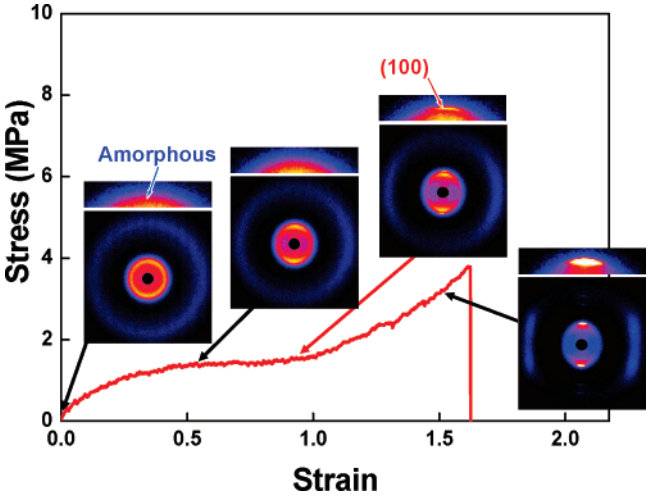

Figure 3. Stress/strain curve recorded at 370 °C with the corresponding change of in situ WAXD patterns for the films prepared from $M_n = 1.0 \times 10^7$ powder. Draw direction on WAXD patterns is horizontal. Enlarged images of the crystalline reflection regions were attached on the upper side.

started in a molten state at 370 °C, which can be confirmed by unoriented amorphous scattering observed in the temperature-equilibrating stage before drawing. This amorphous scattering gradually orients on the equator with continued drawing, as seen in Figure 3. Afterward, a crystal reflection appeared on the equator at the end of the plateau stress region. Chain orientation is higher than that for the solid-drawing in Figure 2. However, the first layer reflections of (107) and (108) reflections were weaker than those for solid-state drawing, due to the activated chain slippage. These results suggest that the oriented crystallization from amorphous chains occurs even while being drawn from the PTFE melt. Considering that the resultant oriented film obtained by subsequent cooling after melt-drawing exhibits a T_m of 335 °C, it could be also said that the drawing at 370 °C may be initiated from the complete molten state exceeding the thermodynamically equilibrium T_m of PTFE.

For quantitative analyses of the changes in the scattering or reflection intensities during drawing, a line profile was extracted along the equator from each in situ WAXD pattern. The obtained series of equatorial profiles was stacked in terms of strain. For the solid-drawing at 300 °C, the intensity of the (100) reflection increased monotonically with strain, but changes in amorphous scattering were less pronounced during the entire strain region, as shown in Figure 4.

In contrast, melt-drawing produced significant changes in both amorphous scattering and crystalline reflection due to oriented crystallization from the melt during drawing. As seen in Figure 5 a, the early stage of melt-drawing at 370 °C exhibited only amorphous scattering around $2\theta = 10°$. However, further drawing produced a (100) reflection that gradually increased. The pronounced growth of crystalline reflection, beginning beyond the critical strain around 0.97, indicates rapid crystallization during drawing. These correlated increases and decreases in the intensities of the amorphous scattering and crystalline reflection during melt-drawing suggest component transformation from an initial amorphous phase to a crystalline phase. To clarify the component changes of amorphous and crystalline phases, the integral intensity of each scattering or reflection was estimated through a peak-resolution analysis of the series of the equatorial profiles presented in Figure 5a. For comparison, the corresponding meridional profiles were also analyzed to estimate the unoriented amorphous component. Figure 5b depicts

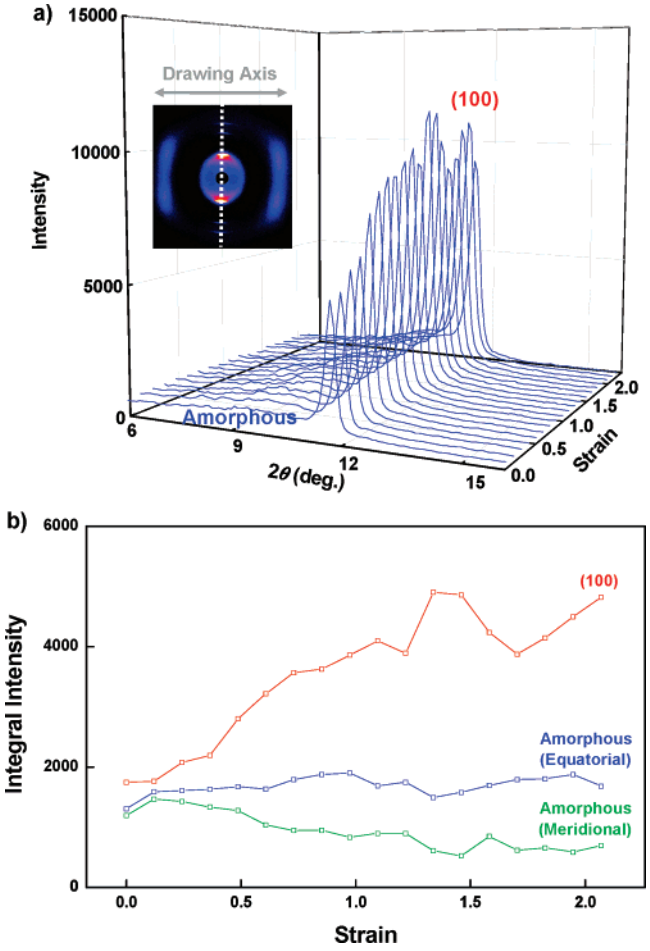

Figure 4. (a) 3-D plot of WAXD line profiles extracted along the equators of the series of in situ WAXD patterns recorded during solid-drawing at 300 °C in Figure 2. The schematic of the equatorial extraction of the profile is indicated by the dotted line with the image in the figure. (b) Comparison of changes in integral intensities estimated from peak resolutions of the equatorial line profiles in part a. Red and blue plots represent pseudo-hexagonal (100) reflection and amorphous scattering. The other integral intensity of the amorphous scattering estimated from a meridional profile is plotted in green.

the changes in the integral intensities of amorphous scattering and crystalline (100) reflection during melt-drawing at 370 °C. The gray shaded area indicates a plateau region in the stress/strain curve in Figure 3. Such a plateau stress region was estimated from the differential plots of the stress/strain curve. The zero-differential region corresponds to the plateau stress region in the original stress/strain curve (see Supporting Information). The difference between the equatorial and meridional amorphous intensities gradually increased when the draw started. This suggests that the amorphous chain orientation is enhanced by melt-drawing. In contrast, the crystalline reflection first appears around the end of the plateau region, and then rapidly increases in intensity as the draw enters the strain-hardening stage. Correspondingly, the intensity of equatorial amorphous scattering maintains a constant level until this critical strain is reached. Specifically, crystallization does not occur in the plateau stress region even though the orientation of the amorphous chain is apparently induced, implying that disentanglement of the molecular chains proceeds before this critical strain.

Resultant Properties. The difference in phase development mechanisms between solid- and melt-drawings of PTFE is reflected in the properties of the resultant oriented films. Table 1 compares the tensile strengths of the films drawn up to three

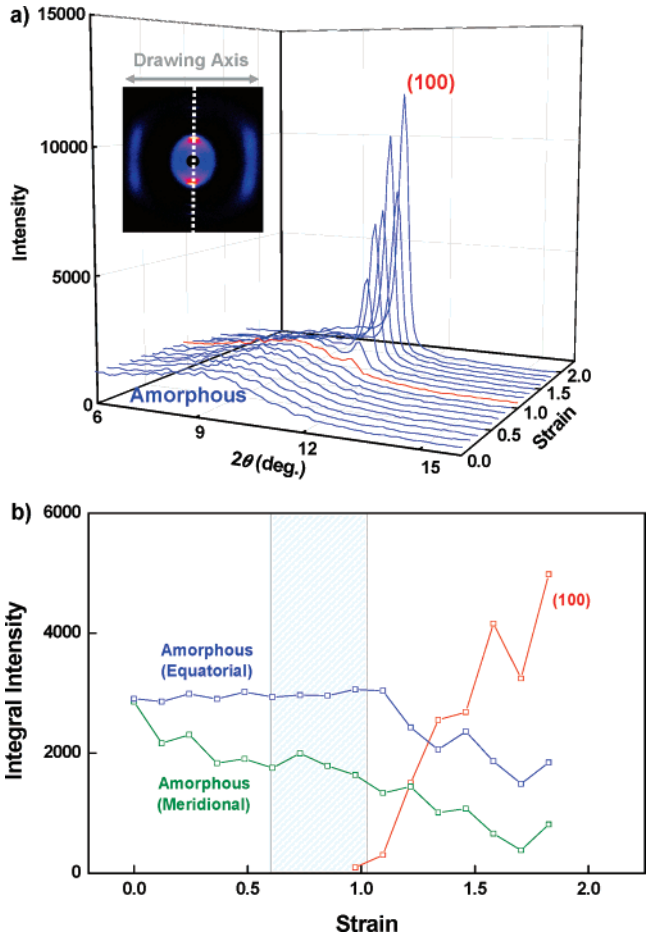

Figure 5. (a) 3-D plot of WAXD line profiles extracted along the equators of the series of in situ WAXD patterns recorded during melt-drawing at 370 °C in Figure 3. The schematic of the equatorial extraction of the profile is represented by the dotted line with the image in the figure. The red profile was obtained at a critical strain of 0.97. (b) Comparison of changes in integral intensities estimated from peak resolutions of the equatorial line profiles in part a. The meanings of plot colors are the same as in Figure 4. Gray shaded area indicates the plateau stress region determined from the stress−strain curve in Figure 3.

times at temperatures ranging from 25 to 390 °C. Drawing temperatures below 300 °C are categorized as solid-drawing; others are melt-drawing. These tensile strengths were measured at room temperature. Stress values recorded at a strain of 1 during drawing at each temperature were also compared. The draw stress decreases with increasing drawing temperature, but the resultant tensile strength significantly increases with reaching the melt-drawing category. It should be noted that these strength values could be underestimated because the chuck easily slipped on these tensile tests at room temperature, due to the low friction coefficient of PTFE. Therefore, the accurate estimation of elongation at break was unsuccessful. Considering the results of the in situ WAXD analyses described above, the origin of the superior properties of melt-drawn film could be possibly ascribed to the prior orientation of the molten chains induced through molecular disentanglement in the plateau stress region.

This discussion suggests that elongation of the plateau stress region will induce further development of the resulting mechanical properties. Therefore, optimization of the melt-drawing conditions was examined. For the drawability of UHMW−PE melt, there is an optimum combination of drawing rate and temperature that gives the highest possible drawability, leading to superior resultant properties.[23] Similar effects of melt-drawing conditions were anticipated for the UHMW−PTFE used in this study. First, the drawing rate dependence was examined with the drawing temperature fixed at 370 °C. The drawing crosshead speed varied from 4 to 100 mm/min, including the standard 24 mm/min adopted in this study. However, no remarkable change in drawing behavior was observed. The recorded lengths of the plateau stress region were almost the same, independent of the drawing rate. In contrast, the drawing temperature significantly affects the plateau stress phenomenon. Figure 6 compares stress/strain curves recorded at 370 to 390 °C with the drawing speed fixed at the standard 24 mm/min. The plateau stress region became more extended with increasing drawing temperature. The enhancement of molecular mobility with increasing temperature facilitates chain relaxation during melt-drawing.

The resultant properties of films melt-drawn at these higher temperatures were measured at room temperature (Table 1). The tensile strength at a draw ratio of 3 increased with increasing drawing temperature even in the melt-drawing category, exhibiting good correlation with the length of the plateau stress region. The maximum achievable tensile strength for the film melt-drawn at 390 °C was 240 MPa. This value is 11 times higher than that of commercial PTFE film (Fluon-PTFE, AGC).

Transparency is another superior characteristic of the melt-drawn PTFE film prepared in this study. The manufacture of PTFE films or sheets usually begins with the reactor powder state. As mentioned above, the high melt viscosity of PTFE prevents adhesion between powder boundaries, even if sintering is performed above T_m. Unfortunately, solid-drawing signifies such powder boundaries, and the resulting void formation whitens the obtained drawn material. In contrast, the lower deformation stress during melt-drawing results in less void formation, yielding superior transparency. Similar results were obtained for melt-drawing of UHMW−PE.[32] The transparency of the PTFE films prepared in this study was evaluated by light transmittance measurements at room temperature. The obtained data are also listed in Table 1. The calculated absorption coefficient exhibits a remarkable difference between melt- and solid-drawing. It should be emphasized that the transparency of PTFE films prepared by melt-drawing is one-ninth of that for the above-mentioned commercial PTFE film. The reduced void formation of the melt-drawn films achieved both high transparency and superior breaking strength.

Generally, the superior mechanical properties and high transparency are contradictory because both are controlled by the increasing or decreasing crystallinity of the prepared film. The achievement of both advantages is characteristic of our PTFE film, prepared by the melt-drawing technique. The maintained adhesion between the powders and subsequent amorphous orientation during melt-drawing are keys to such high performance. The obtained films can be successfully applied as roof membranes for dome stadiums, where utilization of natural sunlight radiation and stability of all building components are required.

Thermal shrinkage tests were also tried for confirmation of molecular disentanglement, but it was unfortunately insufficient. In our previous UHMW−PE studies,[19−21] the complete shrinkage was achieved far above the melt-drawing temperature, i.e., 150 °C-drawn samples were shrunk at 220 °C. In the present study, melt-drawing of UHMW−PTFE was made at 370−390 °C, thus the thermal shrinkage tests should be provided above 420 °C at least, which exceeds the maximum temperature of our high-temperature extension device.

Table 1. Comparison of Draw Stress at a Strain of 1 and Resultant Properties for the Films Drawn up to Three Times at Each Drawing Temperature for the Films Prepared from $M_n = 1.0 \times 10^7$ Powder

	solid-drawing			melt-drawing			commercial film[d]
drawing temp (°C)	25	50	300	370	380	390	
stress at strain of 1 (MPa)[a]	14.3	12.3	3.0	1.5	1.5	1.4	
tensile strength (MPa)[b]	55	60	80	193	202	240	22
absorption coeff (per 1-μm thickness)[c]	0.119	0.140	0.149	0.086	0.075	0.095	0.698

[a] Measured at each drawing temperature. [b] Determined by tensile tests at room temperature. [c] Estimated by transmission measurements using a light with a 430 nm wavelength. [d] Fluon-PTFE, AGC

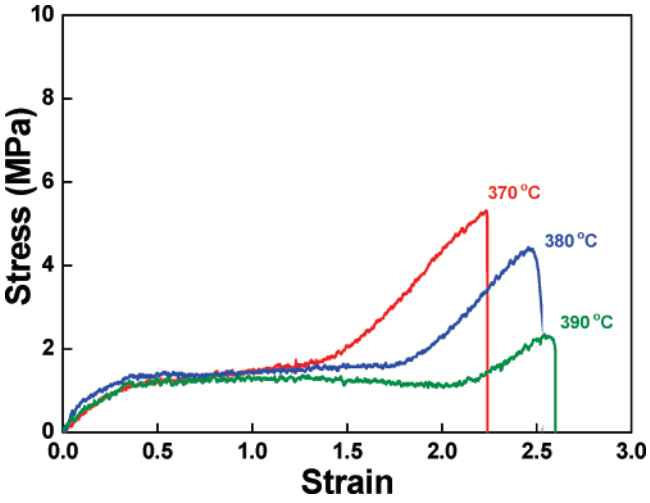

Figure 6. Comparison of stress/strain curves recorded at 370 to 390 °C during drawing of the UHMW−PTFE films prepared from $M_n = 1.0 \times 10^7$ powder.

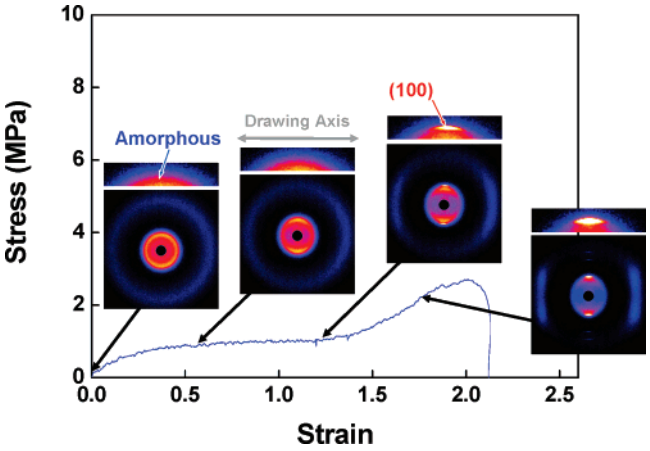

Figure 7. Stress/strain curve recorded at 370 °C with the corresponding change of in situ WAXD patterns for $M_n = 4.0 \times 10^6$ film. Draw direction on WAXD patterns is horizontal. Enlarged images of the crystalline reflection regions were attached on the upper side.

Effect of Molecular Weight on Melt-Drawing Behavior. Such a structural change from random amorphous through oriented amorphous into the final crystalline phase is characteristic of melt-drawing of UHMW materials, including the present PTFE as well as PE. Therefore, the results for different MW PTFEs having $M_n = 4.0 \times 10^6$ and 2.0×10^6 were compared to those obtained for the former $M_n = 1.0 \times 10^7$ sample. The films were prepared from these UHMW−PTFE powders under the same conditions. The in situ WAXD analyses with simultaneous recording of stress/strain curves were carried out for melt-drawing at 370 °C with a CHS of 24 mm/min.

First, the results for the middle $M_n = 4.0 \times 10^6$ film are discussed. Figure 7 depicts the stress/strain curves observed with a series of WAXD patterns recorded at the corresponding strains. The unoriented amorphous scattering was observed before

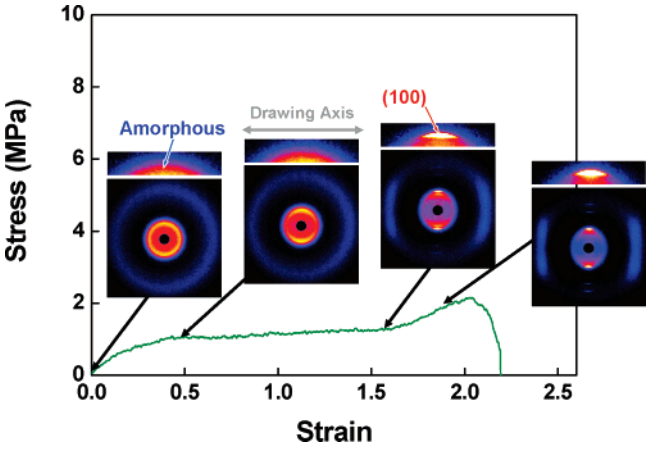

Figure 8. Stress/strain curve recorded at 370 °C with the corresponding change of in situ WAXD patterns for $M_n = 2.0 \times 10^6$ film. Draw direction on WAXD patterns is horizontal. Enlarged images of the crystalline reflection regions were attached on the upper side.

drawing, meaning that the complete molten state was obtained at 370 °C for this middle $M_n = 4.0 \times 10^6$ film, too. It is also a common phenomenon in higher $M_n = 1.0 \times 10^7$ films that the molecular orientation of the amorphous phase is induced in the early stage of melt-drawing. Subsequent oriented crystallization was also observed with entering the strain-hardening region. However, the shape of the corresponding stress/strain curve depends significantly on the sample MW. A comparison of Figures 3 and 7 demonstrates that the length of the plateau region is greater for this middle $M_n = 4.0 \times 10^6$ film than that for the higher $M_n = 1.0 \times 10^7$ film. This trend was further emphasized for the $M_n = 2.0 \times 10^6$ film (Figure 8).

In Figures 7 and 8, the patterns shown near the end of the plateau region were the next ones from the critical strains where oriented crystallization begins. Indeed, crystalline reflections just at the critical strains for these lower MW films were much weaker than the corresponding one for the $M_n = 1.0 \times 10^7$ film (Figure 3). Therefore, the next patterns from the critical strains were shown in these figures to emphasize the oriented crystallization phenomenon. However, the crystalline reflection peaks were clearly seen even just at the critical strains in the equatorial line profiles (see Supporting Information). The component changes of amorphous and crystalline phases were also estimated through a peak-resolution analysis of the series of these equatorial profiles. Independent of the sample MW, only the amorphous scattering peak is recognized at the beginning of drawing. The gradual increase of the difference between the equatorial and meridional amorphous intensities in the early stage of melt-drawing indicates the amorphous orientation. Subsequently, the pseudo-hexagonal (100) reflection becomes observable beyond each critical strain, i.e., 1.1 for the $M_n = 4.0 \times 10^6$ film and 1.5 for the $M_n = 2.0 \times 10^6$ film.

To compare the later oriented crystallization for different MW samples, the integral intensity changes of the pseudo-hexagonal (100) reflection are summarized in Figure 9. The critical strain of starting crystallization increases with decreasing sample MW.

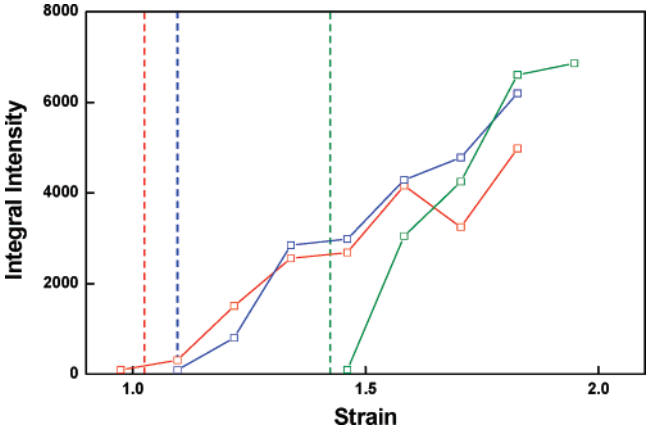

Figure 9. Comparison of changes in integral intensities of pseudo-hexagonal (100) reflection estimated from peak resolutions of the equatorial line profiles. Key: red, $M_n = 1.0 \times 10^7$ film; blue, $M_n = 4.0 \times 10^6$ film; green, $M_n = 2.0 \times 10^6$ film. Dotted lines indicate the end of a plateau region in the stress profiles depicted in Figures 5, 7, and 8.

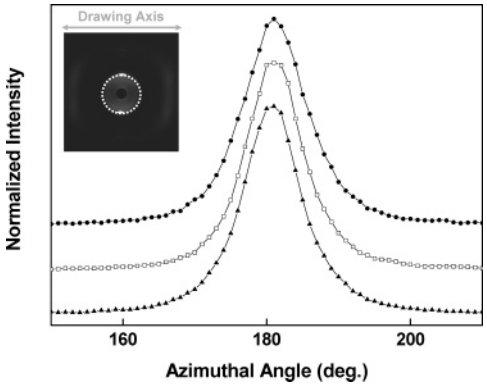

Figure 10. Azimuthal profiles extracted along the azimuthal angle of the in situ WAXD patterns recorded during melt-drawing at 370 °C at the same strain of 1.8. The schematic of azimuthal extraction of the profile is represented by the dotted line with the image in the figure. Line symbols represent the M_n of the films: (●), 1.0×10^7; (○), 4.0×10^6; (▲), 2.0×10^6.

This trend is co-incident with the shift of the end strain of the plateau stress region, indicated by dotted lines in Figure 9. This combination of the critical strain and length of the plateau region implies that the ease of relaxing the amorphous orientation for the lower MW leads to the delay of the later crystallization. Another feature in Figure 9 is the MW dependence of the slope of the plots. The lower MW film yields steeper plots than those of the higher MW film. Correspondingly, the maximum value of the reflection intensity at the highest achievable strain is higher for the lower MW film.

The orientation of the above crystalline reflection was also compared for the different MW films. Azimuthal profiles depicted in Figure 10 were extracted from the in situ WAXD patterns recorded at the same strain of 1.8 for different MW films. This strain is in the strain-hardening region beyond the plateau stress region. The obtained peak shape is almost the same for all films having different MWs. The half-height widths of these peaks were also estimated but exhibit similar values around 10°. These results suggest that the crystalline chain orientation in the final stage of oriented crystallization is independent of the sample MW for melt-drawing of PTFE. Therefore, the difference of the slope of the crystalline intensity plots in Figure 9 is attributed to the crystallinity development during melt-drawing, not to the chain orientation change. This means that the rate of the oriented crystallization is higher for the lower MW once it is initiated by entering the strain-hardening region.

Table 2. Molecular Weight Dependence of Resultant Tensile Strength and Crystallinity for the Films Drawn up to Three Times at 370 °C

M_n	1.0×10^7	4.0×10^6	2.0×10^6
tensile strength (MPa)[a]	193	171	128
crystallinity (%)	46	56	70

[a] Determined by tensile tests at room temperature. [b] Calculated from fusion heat measured by DSC heating scan.

Resultant properties for these different MW samples were also compared. Table 2 summarizes the tensile strength measured at room temperature and crystallinity for the films melt-drawn at 370 °C up to the same draw ratio of 3. The obtained tensile strength decreases with decreasing sample MW. Considering that the lower MW film produced the longer plateau region (Figures 7 and 8), it would be regarded as an index of the ease of the chain disentanglement during melt-drawing. Therefore, the higher crystallinity was achieved for the lower MW film (Table 2), which is consistent with the order of the maximum crystalline intensities (Figure 9). However, the higher content of the chain ends for the lower MW film will reduce the resultant properties, even if the formation of the extended-chain crystals is assumed for our melt-drawing of PTFE.

Conclusion

High-performance PTFE films can be prepared by melt-drawing, utilizing the higher melt-viscosity of PTFE commonly regarded as the cause of its poor processability. The defining characteristic of our melt-drawing process lies in amorphous orientation with possible disentanglement of the molten chains. This unique structural formation provides superior mechanical properties and transparency of the resultant material. In contrast, it was difficult to achieve sufficient orientation of the amorphous component in solid-drawing because deformation in the crystalline state is predominant during drawing below the sample's T_m. These results suggest that melt-drawing is the preferable technique for manufacturing high-performance PTFE films or membranes. The MW effects on melt-drawing behavior and resultant properties of PTFE were also discussed. At the same melt-drawing temperature, the beginning point for oriented crystallization from the melt shifted to the higher strain side with decreasing sample MW. Correspondingly, the crystallization rate was also accelerated, but the obtained properties decreased, possibly due to the higher content of the chain ends.

Acknowledgment. In situ WAXD measurements using synchrotron radiation were performed at SPring-8, Japan Synchrotron Radiation Research Institute (2004A0159-NL2b-np/BL40B2). We appreciate the cooperation of Drs. Sono Sasaki and Katsuaki Inoue (JASRI). This work was partly supported by Industrial Technology Research Grant Program in '04 from the New Energy and Industrial Technology Development Organization (NEDO) of Japan.

Supporting Information Available: Text discussing determination of critical strain and detailed WAXD data analyses for the lower MW films and figures showing differential stress-strain plots, 3-D WAXD plots, and comparisons of changes in the integral intensities. This material is available free of charge via the Internet at http://pubs.acs.org.

References and Notes

(1) Cox, J. M.; Wright, W. W. *J. Appl. Polym. Sci.* **1964**, *8*, 2935.
(2) Gonon, P.; Sylvestre, A. *J. Appl. Phys.* **2002**, *92*, 4584.

(3) Briscoe, B. J.; Ni, Z. *Wear* **1984**, *100*, 221.
(4) Ansile, K. M.; Bachelder, E. M.; Borkar, S.; Zahr, A. S.; Sen, A.; Badding, J. V.; Pishco, M. V. *Langmuir* **2007**, *23*, 747.
(5) Brown, R. G. *J. Chem. Phys.* **1964**, *40*, 2900.
(6) Corradini, P.; De Rosa, C.; Guerra, G.; Petraccone, V. *Macromolecules* **1987**, *20*, 3043.
(7) Corradini, P.; Guerra, G. *Macromolecules* **1977**, *10*, 1410.
(8) De Rosa, C.; Guerra, G.; Petraccone, V.; Centore, R.; Corradini, P. *Macromolecules* **1988**, *21*, 1174.
(9) Kimmig, M.; Strobl, G.; Stuhn, B. *Macromolecules* **1994**, *27*, 2481.
(10) D'Amore, M.; Auriemma, F.; De Rosa, C.; Barone, V. *Macromolecules* **2004**, *37*, 9473.
(11) D'Amore, M.; Talarico, G.; Barone, V. *J. Am. Chem. Soc.* **2006**, *128*, 1099.
(12) Tervoort, T.; Visjager, J.; Graf, B.; Smith, P. *Macromolecules* **2000**, *33*, 6460.
(13) Ochoa, I.; Hatzikiriakos, S. G. *Powder Technol.* **2005**, *153*, 108.
(14) Ochoa, I.; Hatzikiriakos, S. G. *Powder Technol.* **2004**, *146*, 73.
(15) Uehara, H.; Jounai, K.; Endo, R.; Okuyama, H.; Kanamoto, T.; Porter, R. S. *Polym. J.* **1997**, *29*, 198.
(16) Endo, R.; Jounai, K.; Uehara, H.; Kanamoto, T.; Porter, R. S. *J. Polym. Sci., Polym. Phys. Ed.* **1998**, *36*, 2551.
(17) Endo, R.; Kanamoto, T. *J. Polym. Sci., Polym. Phys. Ed.* **2001**, *39*, 1995.
(18) Sawai, D.; Watanabe, D.; Morooka, N.; Kuroki, H.; Kanamoto, T. *J. Polym. Sci., Polym. Phys. Ed.* **2006**, *44*, 3369.
(19) Nakae, M.; Uehara, H.; Kanamoto, T.; Ohama, T.; Porter, R. S. *J. Polym. Sci., Polym. Phys. Ed.* **1999**, *37*, 1921.
(20) Uehara, H.; Nakae, M.; Kanamoto, T.; Zachariades, A. E.; Porter, R. S. *Macromolecules* **1999**, *32*, 2761.
(21) Nakae, M.; Uehara, H.; Kanamoto, T.; Zachariades, A. E.; Porter, R. S. *Macromolecules* **2000**, *33*, 2632.
(22) Uehara, H.; Kakiage, M.; Yamanobe, T.; Komoto, T.; Murakami, S. *Macromol. Rapid Commun.* **2006**, *27*, 966.
(23) Kakiage, M.; Yamanobe, T.; Komoto, T.; Murakami, S.; Uehara, H. *J. Polym. Sci., Polym. Phys. Ed* **2006**, *44*, 2455.
(24) Kakiage, M.; Yamanobe, T.; Komoto, T.; Murakami, S.; Uehara, H. *Polymer* **2006**, *47*, 8053.
(25) Samon, J. M.; Schultz, J. M.; Hsiao, B. S. *Polymer* **2000**, *41*, 2169.
(26) Wu, J.; Schultz, J. M.; Samon, J. M.; Pangelinan, A. B.; Chuah, H. H. *Polymer* **2001**, *42*, 7141.
(27) Wu, J.; Schultz, J. M.; Samon, J. M.; Pangelinan, A. B.; Chuah, H. H. *Polymer* **2001**, *42*, 7161.
(28) Ran, S.; Zong, X.; Fang, D.; Hsiao, B. S.; Chu, B.; Phillips, R. A. *Macromolecules* **2001**, *34*, 2569.
(29) Yeh, F.; Hsiao, B. S.; Sauer, B. B.; Michel, S.; Siesler, H. W. *Macromolecules* **2003**, *36*, 1940.
(30) Chen, X.; Yoon, K.; Burger, C.; Sics, I.; Fang, D.; Hsiao, B. S.; Chu, B. *Macromolecules* **2005**, *38*, 3883.
(31) Li, L.; de Jeu, W. H. *Adv. Polym. Sci.* **2005**, *181*, 75.
(32) Uehara, H.; Yoshida, R.; Kakiage, M.; Yamanobe, T.; Komoto, T. *Ind. Eng. Chem. Res.* **2006**, *45*, 7801.
(33) Suwa, T.; Takehisa, M.; Machi, S. *J. Appl. Polym. Sci.* **1973**, *17*, 3253.
(34) Murakami, S.; Tanno, K.; Tsuji, M.; Kohjiya, S. *Bull. Inst. Cham. Res., Kyoto Univ.* **1995**, *72*, 418.
(35) Murakami, S. *Nippon Kagaku Kaishi* **2000**, *2*, 141.
(36) Lehnert, R. J.; Hendra, P. J.; Everall, N.; Clayden, N. J. *Polymer* **1997**, *38*, 1521.

MA071898G